Vietnam Journal of Earth Sciences, 46(3), 303-321, https://doi.org/10.15625/2615-9783/20400

Vietnam Journal of Earth Sciences
https://vjs.ac.vn/index.php/jse

The present strain rate of Quang Nam - Quang Ngai and the surrounding region

Bui Nhi Thanh[1,2], Tran Van Phong[2,3*], Nguyen Van Diep[1], Phan Trong Trinh[2,3]

[1]*Institute of Marine Geology and Geophysics, VAST, Hanoi, Vietnam*
[2]*Graduate University of Science and Technology, VAST, Hanoi, Vietnam*
[3] *Institute of Geological Sciences, VAST, Hanoi, Vietnam*

Received 23 June 2023; Received in revised form 20 February 2024; Accepted 21 March 2024

ABSTRACT

Studying the present strain rate is significant in determining the characteristics and origin of geological anomalies in the region. Tectonic strain occurs under the influence of various factors, especially tectonic forces, and only a few cases of deformation occur at speeds observable by humans. This research uses velocity data from GNSS measurements in Quang Nam - Quang Ngai and surrounding regions to assess present tectonic strain. The combination of methods used in this study includes calculating the ITRF Earth-fixed frame to minimize errors, the method of relative velocity calculation to compare the speed variations between station positions, and the deformation calculation method using the QOCA software developed by NASA's Jet Propulsion Laboratory (JPL). The calculated results show that the coastal areas of the study have relatively low strain rates with the principal strain rate <15 nano-strain/year, the magnitude of deformation is always less than 7.5 nano-strain/year, and the area is conducive to the development of dominant reverse faulting.

Keywords: Quang Nam, Quang Ngai, present strain rate, tectonic, GNSS.

1. Introduction

Along with economic development, Vietnam suffers many impacts of natural disasters, such as climate change, sea level rise, water pollution, coastal erosion, landslides, earthquakes, and tsunamis (Pham et al., 2023; Dao et al., 2023; Doan et al., 2024; Nguyen et al., 2023). Present tectonic movements in Vietnam have important practical significance in assessing geological hazards in coastal areas. The initial results employing satellite geodesy (GPS) for studying contemporary tectonic displacement and deformation in Southeast Asia were presented by (Tregoning et al., 1994), followed by findings from the GEODYSSEA project documented in publications by (Chamote-Rooke and Pichon, 1999) and (Michel et al., 2001). Recent GPS studies by (Bock et al., 2003) have identified the Sundaland block undergoing independent motion. Numerous studies on Earth's crustal deformation using GPS measurements and seismic data have also been conducted in China (Hu et al., 2007; King et al., 1997; Liao and Wu, 2009; Shen et al., 2005; Wang et al., 2001), Taiwan (Hsu et al., 2009), the Philippines (Gerald et al., 2007; Yu et al.,

*Corresponding author, Email: tphong1617@gmail.com

2011), and Thailand (Iwakuni et al., 2004), and others.

In Vietnam, (Tran and Nguyen, 2004) concluded, based on the analysis of results from GEODYSSEA, that the Vietnamese territory lies within the Sundaland block, with a relatively horizontal movement velocity of approximately 7 mm/year (corresponding to a deformation rate of 15 nano-strain/year or 1,5 $\times 10^{-8}$/year). This value can be considered a limiting threshold for motion in the Indochina region. (Duong, 2005; Duong et al., 2006) Employed the deformation calculation method within individual triangles to assess the lateral movements along the Red River fault and the Lai Châu - Điện Biên fault (Phan, 2010a, b) utilized GPS data collected over four cycles (2007-2010) from the East Sea GPS network to characterize the displacement features in the East Vietnam Sea and its vicinity. The authors calculated deformation and mapped deformation regions based on changes in edge lengths over the measurement period.

(Nguyen, 2012) based on GPS velocity data from the East Sea network and adjacent GPS data, computed and mapped the deformation speed for the entire East Sea region using the deformation calculation method within each polygon, employing the QOCA software for computation (Dong et al., 1998). (Phan, 2013) assessed and mapped the gradient in the Ninh Thuận region and its vicinity using small GPS networks around the proposed locations for constructing two nuclear power plants in Ninh Thuận. The data points were approximately 10 km apart, with a larger grid covering the Ninh Thuận area and its vicinity, where data points were around 50 km apart (Tran, 2016) established and implemented a GPS network in the Khánh Hòa, Ninh Thuận, and nearby regions, integrating geological and geomorphic data. This allowed for a preliminary evaluation of modern tectonic deformation activities and the correlation between modern tectonic deformation and geological-tectonic activities in the area. (Phan et al., 2021, Liem et al., 2021) Constructed a comprehensive observation grid covering the entire East Sea of Vietnam and the mainland to create research maps of modern tectonic deformation rates for the region at a 1:500,000 scale. This is the most recent and detailed study on tectonic displacement and modern tectonic deformation rates for the entire Vietnam mainland and surrounding sea areas.

Due to precision requirements, demands for GNSS data observation time must ensure an adequate duration, and the density of observation points must be sufficient for detailed and reliable results. This poses a challenge because current studies on tectonic deformation rates in the country tend to be localized and not continuous. Recent studies employ the interpolation method for the modern tectonic displacement field to resolve the limitations. This method synthesizes displacement results statistically from previously published materials to calculate the modern tectonic deformation rates for the study area. In this research, we apply a 0.2°× 0.2° interpolation grid for displacement rates to calculate the tectonic strain rates in the study area.

2. Data and Methodology

2.1. Data used

To calculate the present tectonic strain rates for the Quang Nam and surrounding regions, we utilized displacement velocity data from 34 points (Fig. 1, Table 1). These data represent tectonic displacement rates obtained from processing GPS data collected from various sources, including the State-level independent project with codes NT 03/2012 and 02/2012, the Tay Nguyen 3 Program with code TN3/T06, and the PCGIAP project

(Phan et al., 2015a; Phan et al., 2015b; Phan et al., 2015c). Data from the national project, KC.09.22/16-20, were also incorporated (Phan et al., 2021). These measurements were computed in different International Terrestrial Reference Frames (ITRF), so the authors used the NOAA's Horizontal Time-Dependent Positioning (HTDP) software to convert the data from various ITRF Earth reference frames to a standardized frame, ITRF2008 (Pearson et al., 2010). The data includes the following components: VE (mm/year) - Eastward displacement component velocity, VN (mm/year) - Northward displacement component velocity, SE (mm/year) - Eastward displacement component velocity error, SN (mm/year) - Northward displacement component velocity error. The Pliocene-present fault maps are utilized to interpret the results of strain rate based on a dataset of National research project code KC.09.22/16-20 (Phan et al., 2021) (Fig. 9).

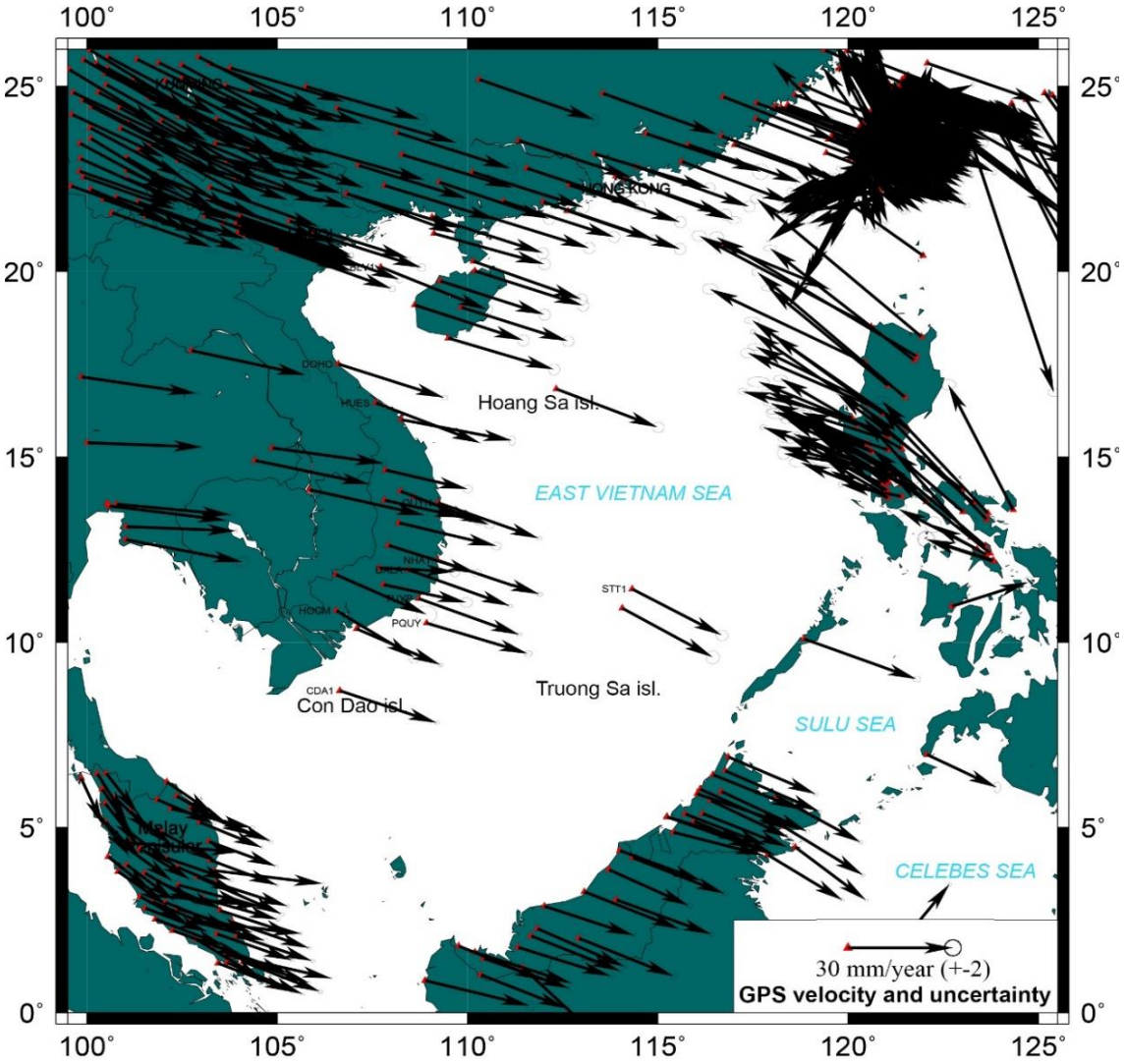

Figure 1. Present Tectonic Displacement Velocity Field in the Study Area and Surrounding Regions

Table 1. The tectonic displacement velocity points are used to calculate the present tectonic strain rates in Quang Nam and the surrounding regions

No	Station	Longitude	Latitude	VE	VN	SE	SN	Sources	Frame
1	CDA1	106.651	8.6915	27.77	-9.46	0.6	0.4	(Phan, 2021)	IGS08
2	DALA	108.445	11.952	29	-10.59	0.7	0.4	(Phan, 2021)	IGS08
3	DOHO	106.615	17.507	30.38	-9.92	0.8	0.6	(Phan, 2021)	IGS08
4	NHAT	109.214	12.207	29.2	-10.07	0.7	0.5	(Phan, 2021)	IGS08
5	PQUY	108.931	10.516	28.97	-8.91	1	0.7	(Phan, 2021)	IGS08
6	QUYN	109.226	13.765	28.88	-10.48	0.7	0.5	(Phan, 2021)	IGS08
7	TUYP	108.715	11.180	28.87	-10.61	0.7	0.4	(Phan, 2021)	IGS08
8	BLV1	107.723	20.128	30.39	-12.49	1.36	1.29	(Phan, 2010a, b)	IGS08
9	STT1	114.331	11.429	25.67	-13.59	1.44	1.34	(Phan, 2010a, b)	IGS08
10	HOCM	106.56	10.849	22.29	-13.77	1.47	1.36	(Phan, 2010a, b)	IGS08
11	HUES	107.593	16.459	29.99	-11.83	0.1	0.1	(Phan, 2010a, b)	IGS08
12	JB21	110.306	25.186	33.14	-11.83	0.7	1.5	(Liao and Wu, 2009)	IGS08
13	BTS3	121.963	20.438	-38.25	27.84	0.9	0.6	(Yu et al., 2011)	IGS08
14	S102	121.558	22.037	-38.54	39.24	0.3	0.3	(Yu et al., 2011)	IGS08
15	KUNM	102.797	25.03	30.92	-17.8	0.8	0.79	(Phan, 2021)	IGS08
16	ZAMB	122.073	6.973	20.07	-9.71	0.84	1.35	(Simons et al., 2007)	IGS08
17	ILOI	122.732	10.968	21.86	7.11	1.13	1.4	(Simons et al., 2007)	IGS08
18	PUER	118.851	10.086	32.13	-11.82	1	0.7	(Simons et al., 2007)	IGS08
19	TABA	108.891	0.863	29.95	-7.4	0.95	1.26	(Simons et al., 2007)	IGS08
20	NNKI	102.747	17.865	32.72	-7.18	0.96	1.53	(Dawson and Hu, 2010)	IGS08
21	HKFN	114.138	22.494	31.28	-11.95	1.6	0.8	(Dawson and Hu, 2010)	IGS08
22	QION	109.845	19.029	30.49	-9.89	1.4	1.3	(Hao et al., 2019)	IGS08
23	YONG	112.335	16.834	29.12	-11.3	1.4	1.3	(Hao et al., 2019)	IGS08
24	F008	114.062	10.913	25.94	-14.42	1.6	1.6	(Hao et al., 2019)	IGS08
25	TNSM	116.725	20.703	30.67	-12.96	0.2	0.2	(Hao et al., 2019)	IGS08
26	BRG1	120.601	18.52	-49.24	26.7	1.72	1.32	(Hao et al., 2019)	IGS08
27	PIMO	121.078	14.636	-30.25	5	1.5	1.4	(Hao et al., 2019)	IGS08
28	XIAM	118.083	24.45	32.37	-12.54	1.3	1.3	(Hao et al., 2019)	IGS08
29	TNML	120.987mai	24.798	30.55	-9.28	1.2	1.2	(Hao et al., 2019)	IGS08
30	KUDA	116.848	6.898	25.13	-10.96	0.42	0.34	(Phan, 2021)	IGS08
31	MIRI	114.002	4.372	23.5	-8.94	0.43	0.34	(Phan, 2021)	IGS08
32	KUAL	103.139	5.319	18.53	-7.56	0.45	0.34	(Phan, 2021)	IGS08
33	MUKA	112.02	2.873	25.62	-8.62	0.47	0.37	(Phan, 2021)	IGS08
34	TGPG	104.108	1.367	21.99	-8.77	0.62	0.47	(Phan, 2021)	IGS08

Note: VE (mm/year) - Eastward displacement component velocity; VN (mm/ year) - Northward displacement component velocity; SE (mm/ year) - Eastward displacement component velocity error; SN (mm/ year) - Northward displacement component velocity error

We use a velocity field with GPS points relatively evenly distributed within the grid to calculate the strain rate. The authors conducted velocity interpolation using a 0.2×0.2 degree grid for the study area based on the displacement rates of 34 selected points, combined with the integration of appropriate velocity fields from the publications of (Hao et al., 2019) and (Mustafar et al., 2017) (Fig. 1). Interpolation was carried out using the Kriging method (Isaaks and Srivastava, 1989), utilizing Surfer 12.0 software (Golden Software, Inc.) for each velocity component.

Kriging is an interpolation method that identifies the typical characteristics of an entire surface represented by measured values and applies those characteristics to other parts

of the surface. Kriging is based on the "surface analysis" and "weighted average" methods. "Surface analysis" determines a mathematical equation describing the general trend of the surface but does not account for local irregularities. Local interpolation is used to calculate deviations from the global trend due to the irregularities of the region. The "weighted average" method is used to calculate this variation. The trend of the deviations between the global surface curve and the observation points determines the weights. The result is an evenly distributed displacement velocity field. Figure 1 introduces the obtained displacement velocity field and actual measured velocity vectors.

Strain rate calculations were done for a 0.2×0.2° grid using this displacement velocity field (Fig. 2). The diagram illustrates that the study area exhibits a uniform east-southeast displacement direction with an average velocity of 31 mm/year.

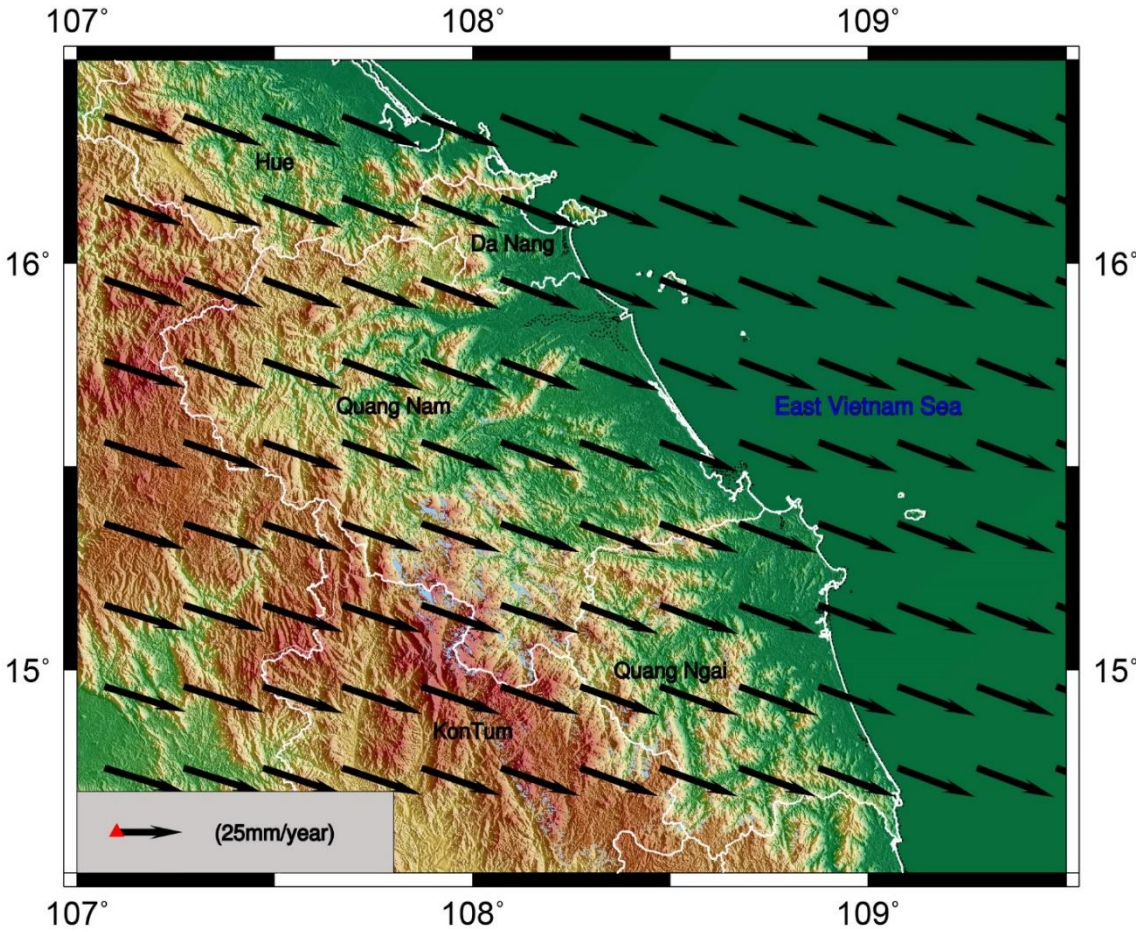

Figure 2. Interpolated present tectonic displacement velocity field on a 0.2°×0.2° grid in the Quang Nam -Quang Ngai and surrounding regions used for calculating present strain rates

2.2. Methodology

2.2.1. Strain rate calculation

The principles and formulas for calculating strain rate are detailed in (Dong et al., 1998), and the QOCA theory is at the link: https://qoca.jpl.nasa.gov/theory/theory.html. The computational process flow chart is presented in Fig. 3.

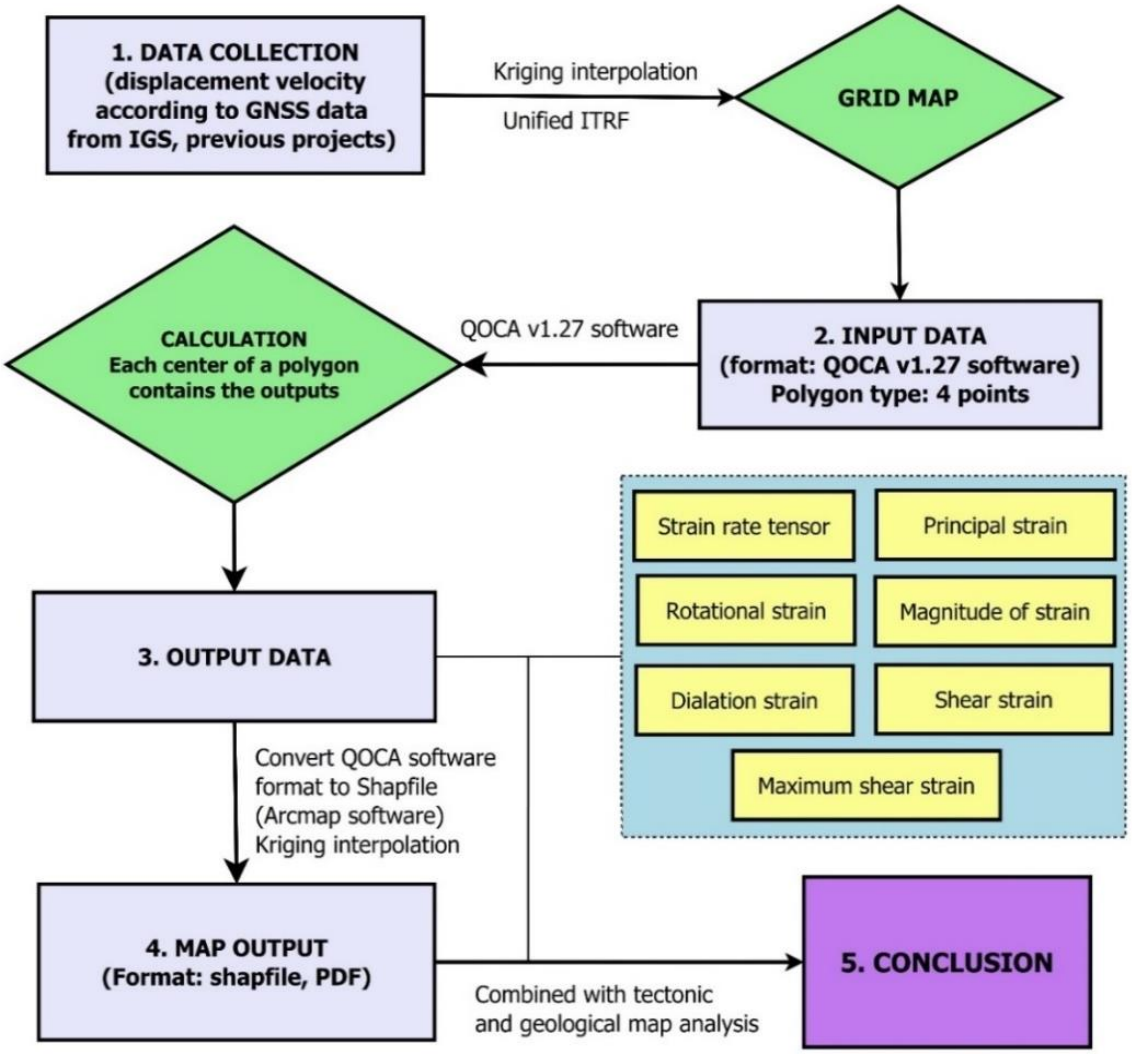

Figure 3. Flow chart of the strain rate calculation

2.2.2. Method for Computing Referenced Frame Transformation

Absolute displacement rate data is processed and computed within the International Terrestrial Reference Frame (ITRF). Over time, the ITRF is continually refined in terms of parameters and technology to achieve the most accurate computation of displacement rates. The latest version is the ITRF2008. However, due to variations in the

choice of the reference frame for processing absolute displacement velocity data in research conditions, there is no consensus on using a unified International Terrestrial Reference Frame (ITRF). To address this issue and eliminate calculation errors associated with different reference frames, NOAA has researched and developed the HTDP software package to compute transformations between various reference frames uniformly. A 7-parameter coordinate frame transformation is employed for the parameter conversion method, provided by the National Institute of Geographic and Forest Information of France (Pearson et al., 2010).

3. Results

The strain rate is computed using the QOCA software (Dong et al., 1998) with input data consisting of the absolute displacement rates of GPS points. The results yield two fundamental strain rates: the principal strain velocity and the rotation strain velocity. Additionally, the velocity field interpolation enables the calculation of several other quantities characteristic of strain, including the magnitude of strain, the magnitude of two-dimensional tensile strain, and the maximum shear strain magnitude.

3.1. Principal Strain rate

As introduced earlier, the principal strain rate is deformation represented in a reference frame where the shear strain rate is zero, and the other two strain rate components are maximized. These two components are the maximum and minimum principal strain rates in this case. The two principal strain rate axes are always perpendicular to each other. The orientation angle θ is the angle between the direction of the minimum principal strain axis and the north direction. By convention, the tensile strain rate is positive, and the compressive strain rate is negative.

The results of calculating the principal strain velocity in the interpolated quadrilateral grid show that the primary influence in the study area is dominated by a compressive strain rate state with high magnitudes concentrated in the western part of the study area and lowest near the coastal strip. The compressive axis on the mainland predominantly trends northeast-southwest, while along the coastline, it shows an opposing tendency. The compressive axes trending northwest-southeast are dominant and have lower magnitudes. Regarding the magnitude of the principal strain velocity within the individual polygons, it typically falls below 15 nano-strain/year (Fig. 4, Table 2).

Table 2. Principal Strain rate and Rotation Rate from the present Displacement Velocity Grid in the Quang Nam - Quang Ngai and surrounding regions

LON	LAT	EPS1	EPS1SIG	EPS2	EPS2SIG	CW-SPIN	SPINSIG	THETA	THETASIG
107.971	14.457	-1.72E-09	4.52E-11	-8.62E-09	4.61E-11	4.17E-09	3.23E-11	74.15	0.2679
108.172	14.457	-2.18E-09	4.51E-11	-7.88E-09	4.63E-11	3.59E-09	3.23E-11	77.0535	0.3252
108.372	14.457	-2.45E-09	4.51E-11	-7.46E-09	4.61E-11	3.21E-09	3.23E-11	82.1544	0.3691
108.573	14.457	-2.57E-09	4.51E-11	-6.59E-09	4.64E-11	2.88E-09	3.23E-11	87.0994	0.4611
108.773	14.457	-2.55E-09	4.51E-11	-6.11E-09	4.64E-11	2.70E-09	3.23E-11	92.8476	0.5205
108.973	14.457	-2.41E-09	4.51E-11	-5.46E-09	4.61E-11	2.64E-09	3.23E-11	98.3831	0.6057
109.174	14.457	-2.12E-09	4.52E-11	-4.71E-09	4.63E-11	2.56E-09	3.23E-11	105.2069	0.7145
109.374	14.457	3.51E-10	4.60E-11	-4.21E-09	4.52E-11	5.19E-09	3.23E-11	-19.6987	0.4049
109.575	14.457	-1.04E-09	4.57E-11	-7.94E-09	4.58E-11	4.97E-09	3.23E-11	133.2696	0.2685
109.775	14.457	-8.29E-10	4.59E-11	-3.00E-09	4.54E-11	4.06E-09	3.23E-11	-31.5259	0.8506
109.976	14.457	-1.33E-09	4.51E-11	-3.36E-09	4.63E-11	2.93E-09	3.23E-11	99.8904	0.909
110.176	14.457	-1.28E-09	4.51E-11	-4.40E-09	4.61E-11	3.02E-09	3.23E-11	89.8973	0.5929
110.377	14.457	-8.52E-10	4.51E-11	-4.75E-09	4.64E-11	2.89E-09	3.23E-11	95.5105	0.475
107.971	14.657	-2.37E-09	4.53E-11	-9.09E-09	4.60E-11	3.93E-09	3.23E-11	68.3723	0.2752
108.172	14.657	-2.80E-09	4.52E-11	-7.99E-09	4.63E-11	3.31E-09	3.24E-11	71.2048	0.3569

LON	LAT	EPS1	EPS1SIG	EPS2	EPS2SIG	CW-SPIN	SPINSIG	THETA	THETASIG
108.372	14.657	-3.03E-09	4.52E-11	-7.32E-09	4.61E-11	2.89E-09	3.23E-11	76.9409	0.4314
108.573	14.657	-3.03E-09	4.51E-11	-6.40E-09	4.64E-11	2.63E-09	3.24E-11	83.8946	0.5493
108.773	14.657	-2.85E-09	4.51E-11	-5.87E-09	4.64E-11	2.45E-09	3.24E-11	91.4151	0.6139
108.973	14.657	-2.54E-09	4.51E-11	-5.25E-09	4.62E-11	2.38E-09	3.23E-11	98.1139	0.6817
109.174	14.657	3.22E-10	4.62E-11	-4.73E-09	4.53E-11	5.16E-09	3.24E-11	-21.492	0.3668
109.374	14.657	7.59E-10	4.60E-11	-4.85E-09	4.53E-11	5.60E-09	3.23E-11	-22.7801	0.33
109.575	14.657	-1.36E-09	4.52E-11	-7.37E-09	4.63E-11	2.08E-09	3.24E-11	109.2617	0.3086
109.775	14.657	-9.35E-10	4.53E-11	-3.47E-09	4.60E-11	2.86E-09	3.23E-11	115.7745	0.7294
109.976	14.657	-7.34E-10	4.52E-11	-3.75E-09	4.63E-11	3.08E-09	3.24E-11	105.7279	0.6145
110.1765	14.6577	-4.15E-10	4.51E-11	-4.28E-09	4.62E-11	3.47E-09	3.23E-11	100.3144	0.4784
110.377	14.6577	1.11E-10	4.52E-11	-5.04E-09	4.64E-11	2.99E-09	3.24E-11	102.2809	0.3598
107.9715	14.8582	-6.62E-09	4.51E-11	-7.46E-09	4.62E-11	6.51E-09	3.23E-11	98.6044	2.1946
108.172	14.8582	-5.35E-09	4.58E-11	-8.26E-09	4.58E-11	6.41E-09	3.24E-11	134.6447	0.6355
108.3725	14.8582	-3.81E-09	4.57E-11	-9.24E-09	4.56E-11	6.44E-09	3.23E-11	-41.6862	0.3403
108.573	14.8582	-2.41E-09	4.59E-11	-1.00E-08	4.57E-11	6.62E-09	3.24E-11	-40.6153	0.2433
108.773	14.8582	-1.15E-09	4.59E-11	-1.07E-08	4.57E-11	6.92E-09	3.24E-11	-40.027	0.1947
108.9735	14.8582	-2.99E-11	4.58E-11	-1.12E-08	4.55E-11	7.29E-09	3.23E-11	-39.5375	0.1657
109.174	14.8582	4.62E-10	4.62E-11	-6.17E-09	4.54E-11	5.86E-09	3.24E-11	-28.275	0.2795
109.3745	14.8582	-1.39E-09	4.55E-11	-4.18E-09	4.58E-11	2.91E-09	3.23E-11	127.1899	0.6638
109.575	14.8582	-1.15E-09	4.52E-11	-8.45E-09	4.63E-11	1.75E-09	3.24E-11	107.8567	0.254
109.7755	14.8582	-1.32E-09	4.52E-11	-3.37E-09	4.61E-11	2.18E-09	3.23E-11	109.1701	0.8994
109.976	14.8582	-7.39E-10	4.52E-11	-3.31E-09	4.63E-11	2.34E-09	3.24E-11	107.9844	0.7202
110.1765	14.8582	8.96E-11	4.51E-11	-3.93E-09	4.62E-11	2.88E-09	3.23E-11	101.0656	0.4597
110.377	14.8582	5.77E-10	4.51E-11	-5.12E-09	4.64E-11	2.88E-09	3.24E-11	101.6416	0.3253
107.9715	15.0586	-2.99E-09	4.56E-11	-9.06E-09	4.58E-11	3.33E-09	3.23E-11	49.2449	0.3048
108.172	15.0586	-3.60E-09	4.57E-11	-7.47E-09	4.59E-11	2.88E-09	3.24E-11	49.9167	0.4789
108.3725	15.0586	-4.01E-09	4.55E-11	-5.93E-09	4.58E-11	2.55E-09	3.23E-11	52.2867	0.9629
108.573	15.0586	-4.16E-09	4.52E-11	-4.75E-09	4.64E-11	2.39E-09	3.24E-11	75.1012	3.1452
108.773	15.0586	-3.40E-09	4.55E-11	-4.42E-09	4.61E-11	2.39E-09	3.24E-11	120.5541	1.8102
108.9735	15.0586	-2.42E-09	4.55E-11	-4.43E-09	4.59E-11	2.43E-09	3.23E-11	126.0838	0.9211
109.174	15.0586	-1.97E-09	4.53E-11	-6.37E-09	4.63E-11	2.24E-09	3.24E-11	110.8398	0.4211
109.3745	15.0586	-1.17E-09	4.55E-11	-3.85E-09	4.59E-11	2.39E-09	3.23E-11	126.1575	0.6894
109.575	15.0586	-9.09E-10	4.52E-11	-9.16E-09	4.64E-11	1.31E-09	3.24E-11	107.0653	0.225
109.7755	15.0586	-5.31E-10	4.52E-11	-4.20E-09	4.61E-11	2.27E-09	3.23E-11	108.9582	0.5049
109.976	15.0586	-3.14E-10	4.52E-11	-3.21E-09	4.64E-11	1.78E-09	3.24E-11	105.8567	0.6406
110.1765	15.0586	-9.11E-10	4.51E-11	-3.32E-09	4.63E-11	2.35E-09	3.23E-11	95.0191	0.769
110.377	15.0586	-6.46E-10	4.53E-11	-4.16E-09	4.63E-11	2.64E-09	3.24E-11	110.6847	0.5275
107.9715	15.2591	-2.92E-09	4.58E-11	-9.51E-09	4.56E-11	2.60E-09	3.23E-11	41.3438	0.2809
108.172	15.2591	-3.45E-09	4.60E-11	-7.64E-09	4.57E-11	2.11E-09	3.24E-11	39.3892	0.4428
108.3725	15.2591	-3.81E-09	4.59E-11	-5.87E-09	4.55E-11	1.74E-09	3.23E-11	37.5772	0.8967
108.573	15.2591	-3.90E-09	4.60E-11	-4.36E-09	4.57E-11	1.57E-09	3.24E-11	39.6754	4.0426
108.773	15.2591	-3.14E-09	4.56E-11	-3.80E-09	4.60E-11	1.64E-09	3.24E-11	127.9669	2.8288
108.9735	15.2591	-2.10E-09	4.56E-11	-3.81E-09	4.58E-11	1.78E-09	3.23E-11	130.2885	1.0866
109.174	15.2591	-1.54E-09	4.53E-11	-6.21E-09	4.64E-11	1.58E-09	3.24E-11	111.1627	0.3979
109.3745	15.2591	-6.99E-10	4.53E-11	-3.83E-09	4.61E-11	1.88E-09	3.23E-11	116.9414	0.5922
109.575	15.2591	1.93E-10	4.52E-11	-9.08E-09	4.64E-11	5.63E-10	3.24E-11	105.8669	0.2002
109.7755	15.2591	4.11E-10	4.52E-11	-3.98E-09	4.62E-11	2.23E-09	3.23E-11	109.5229	0.4221
109.976	15.2591	6.00E-10	4.53E-11	-4.25E-09	4.63E-11	2.55E-09	3.24E-11	111.5882	0.383
110.1765	15.2591	6.54E-10	4.51E-11	-3.24E-09	4.63E-11	3.01E-09	3.23E-11	103.0428	0.4757
110.377	15.2591	1.03E-09	4.52E-11	-3.46E-09	4.65E-11	2.35E-09	3.24E-11	103.9117	0.413
107.9715	15.4596	-2.90E-09	4.60E-11	-9.58E-09	4.55E-11	1.97E-09	3.23E-11	33.2898	0.2772
108.172	15.4596	-3.39E-09	4.63E-11	-7.41E-09	4.54E-11	1.54E-09	3.24E-11	28.3698	0.4626
108.3725	15.4596	-3.64E-09	4.63E-11	-5.55E-09	4.52E-11	1.25E-09	3.23E-11	14.6538	0.9689
108.573	15.4596	-3.26E-09	4.64E-11	-4.60E-09	4.52E-11	1.27E-09	3.24E-11	-17.9244	1.3855
108.773	15.4596	-2.16E-09	4.61E-11	-4.23E-09	4.56E-11	1.44E-09	3.24E-11	-35.1941	0.9014
108.9735	15.4596	-1.83E-09	4.56E-11	-3.96E-09	4.58E-11	1.37E-09	3.23E-11	129.3541	0.8696
109.174	15.4596	-8.50E-10	4.53E-11	-5.75E-09	4.63E-11	7.01E-10	3.24E-11	114.1107	0.3788
109.3745	15.4596	-4.76E-12	4.54E-11	-3.90E-09	4.61E-11	1.72E-09	3.23E-11	118.2096	0.4759
109.575	15.4596	4.30E-10	4.55E-11	-7.95E-09	4.62E-11	2.56E-09	3.24E-11	121.7272	0.2217
109.7755	15.4596	5.85E-10	4.54E-11	-7.67E-09	4.61E-11	2.70E-09	3.23E-11	119.0817	0.2243

LON	LAT	EPS1	EPS1SIG	EPS2	EPS2SIG	CW-SPIN	SPINSIG	THETA	THETASIG
109.976	15.4596	9.20E-10	4.52E-11	-4.43E-09	4.65E-11	1.70E-09	3.24E-11	103.5555	0.3474
110.1765	15.4596	1.12E-09	4.51E-11	-3.41E-09	4.63E-11	2.00E-09	3.23E-11	95.3747	0.4092
110.377	15.4596	1.40E-09	4.51E-11	-3.25E-09	4.66E-11	1.97E-09	3.24E-11	98.1252	0.399
107.9715	15.66	-2.53E-09	4.61E-11	-9.55E-09	4.54E-11	1.03E-09	3.24E-11	26.6878	0.264
108.172	15.66	-2.86E-09	4.65E-11	-7.22E-09	4.53E-11	4.98E-10	3.24E-11	19.3922	0.4269
108.3725	15.66	-2.81E-09	4.64E-11	-5.27E-09	4.51E-11	2.43E-10	3.24E-11	4.6505	0.7564
108.573	15.66	-2.41E-09	4.65E-11	-4.10E-09	4.53E-11	3.20E-10	3.24E-11	-19.3285	1.1003
108.773	15.66	-1.36E-09	4.60E-11	-3.55E-09	4.57E-11	3.67E-10	3.24E-11	-39.5713	0.8483
108.9735	15.66	-1.02E-09	4.54E-11	-3.85E-09	4.61E-11	7.30E-10	3.24E-11	117.7517	0.6563
109.174	15.66	1.40E-10	4.54E-11	-5.31E-09	4.63E-11	1.98E-10	3.24E-11	117.632	0.3409
109.3745	15.66	5.74E-10	4.54E-11	-3.38E-09	4.61E-11	1.32E-09	3.24E-11	120.5709	0.4687
109.575	15.66	1.07E-09	4.54E-11	-3.67E-09	4.63E-11	1.65E-09	3.24E-11	116.3434	0.3925
109.7755	15.66	1.50E-09	4.52E-11	-1.00E-08	4.63E-11	1.16E-10	3.24E-11	105.5145	0.161
109.976	15.66	1.36E-09	4.52E-11	-4.27E-09	4.65E-11	1.78E-09	3.24E-11	106.5895	0.3301
110.1765	15.66	1.33E-09	4.52E-11	-3.61E-09	4.63E-11	2.89E-09	3.24E-11	108.395	0.3751
110.377	15.66	1.48E-09	4.53E-11	-3.81E-09	4.65E-11	2.72E-09	3.24E-11	108.3283	0.3519
107.9715	15.8605	-2.20E-09	4.63E-11	-9.13E-09	4.52E-11	1.67E-11	3.24E-11	18.4545	0.2675
108.172	15.8605	-2.20E-09	4.67E-11	-6.43E-09	4.51E-11	-4.26E-10	3.24E-11	6.5582	0.4394
108.3725	15.8605	-1.73E-09	4.64E-11	-4.76E-09	4.51E-11	-4.62E-10	3.24E-11	-12.4373	0.6111
108.573	15.8605	-9.84E-10	4.62E-11	-3.95E-09	4.55E-11	-2.55E-10	3.24E-11	-31.829	0.6264
108.773	15.8605	1.09E-10	4.60E-11	-3.65E-09	4.58E-11	5.92E-11	3.24E-11	-41.6543	0.4949
108.9735	15.8605	3.04E-10	4.55E-11	-4.03E-09	4.60E-11	7.34E-10	3.24E-11	124.9532	0.4281
109.174	15.8605	1.44E-09	4.55E-11	-5.35E-09	4.63E-11	4.07E-10	3.24E-11	120.9341	0.2736
109.3745	15.8605	1.60E-09	4.55E-11	-3.46E-09	4.60E-11	1.47E-09	3.24E-11	123.8132	0.3668
109.575	15.8605	1.68E-09	4.55E-11	-3.77E-09	4.63E-11	1.75E-09	3.24E-11	120.4686	0.341
109.7755	15.8605	1.96E-09	4.52E-11	-1.10E-08	4.63E-11	5.92E-10	3.24E-11	108.8084	0.1434
109.976	15.8605	1.98E-09	4.54E-11	-3.86E-09	4.64E-11	2.64E-09	3.24E-11	116.5617	0.3181
110.1765	15.8605	1.76E-09	4.53E-11	-3.62E-09	4.62E-11	3.41E-09	3.24E-11	114.4081	0.3452
110.377	15.8605	1.87E-09	4.54E-11	-4.41E-09	4.64E-11	3.51E-09	3.24E-11	114.7445	0.2961
107.9715	16.061	-1.42E-09	4.65E-11	-7.95E-09	4.51E-11	-1.26E-09	3.24E-11	6.4112	0.2841
108.172	16.061	-8.81E-10	4.67E-11	-5.38E-09	4.51E-11	-1.38E-09	3.25E-11	-10.1861	0.4135
108.3725	16.061	-3.13E-11	4.63E-11	-4.19E-09	4.53E-11	-9.51E-10	3.24E-11	-24.3235	0.4458
108.573	16.061	7.84E-10	4.62E-11	-4.02E-09	4.57E-11	-6.23E-10	3.25E-11	-36.4584	0.3869
108.773	16.061	1.64E-09	4.60E-11	-3.64E-09	4.58E-11	-2.52E-11	3.25E-11	-40.8903	0.352
108.9735	16.061	1.59E-09	4.56E-11	-4.07E-09	4.59E-11	6.12E-10	3.24E-11	128.679	0.328
109.174	16.061	2.43E-09	4.56E-11	-5.44E-09	4.62E-11	3.03E-10	3.25E-11	122.913	0.2365
109.3745	16.061	2.70E-09	4.55E-11	-3.35E-09	4.60E-11	1.57E-09	3.24E-11	124.4822	0.3071
109.575	16.061	2.97E-09	4.55E-11	-3.71E-09	4.63E-11	2.00E-09	3.25E-11	121.0786	0.2784
109.7755	16.061	3.21E-09	4.52E-11	-1.11E-08	4.63E-11	6.51E-10	3.24E-11	109.4841	0.1301
109.976	16.061	3.10E-09	4.54E-11	-3.43E-09	4.64E-11	2.77E-09	3.25E-11	115.034	0.2846
110.1765	16.061	2.78E-09	4.53E-11	-3.15E-09	4.63E-11	3.54E-09	3.24E-11	112.6198	0.3128
110.377	16.061	2.77E-09	4.53E-11	-3.88E-09	4.65E-11	3.64E-09	3.25E-11	112.7527	0.2799

Note: LON: Central longitude of the polygon (degrees); LAT: Central latitude of the polygon (degrees); EPS1: Maximum principal strain rate (strain/year); EPS1SIG: Uncertainty in the determination of maximum principal strain rate (strain/year); EPS2: Minimum principal strain rate (strain/year); EPS2SIG: Uncertainty in the determination of minimum principal strain rate (strain/year); CW-SPIN: Clockwise (positive values) and counterclockwise (negative values) rotation rate (radian/year); SPINSIG: Uncertainty in the determination of rotation rate (radian/year); THETA: Angle between the direction of the minimum principal strain and the north (degrees); THETASIG: Uncertainty in the determination of the THETA angle (degrees); TRIANGLE: Name of the polygon in the strain rate grid

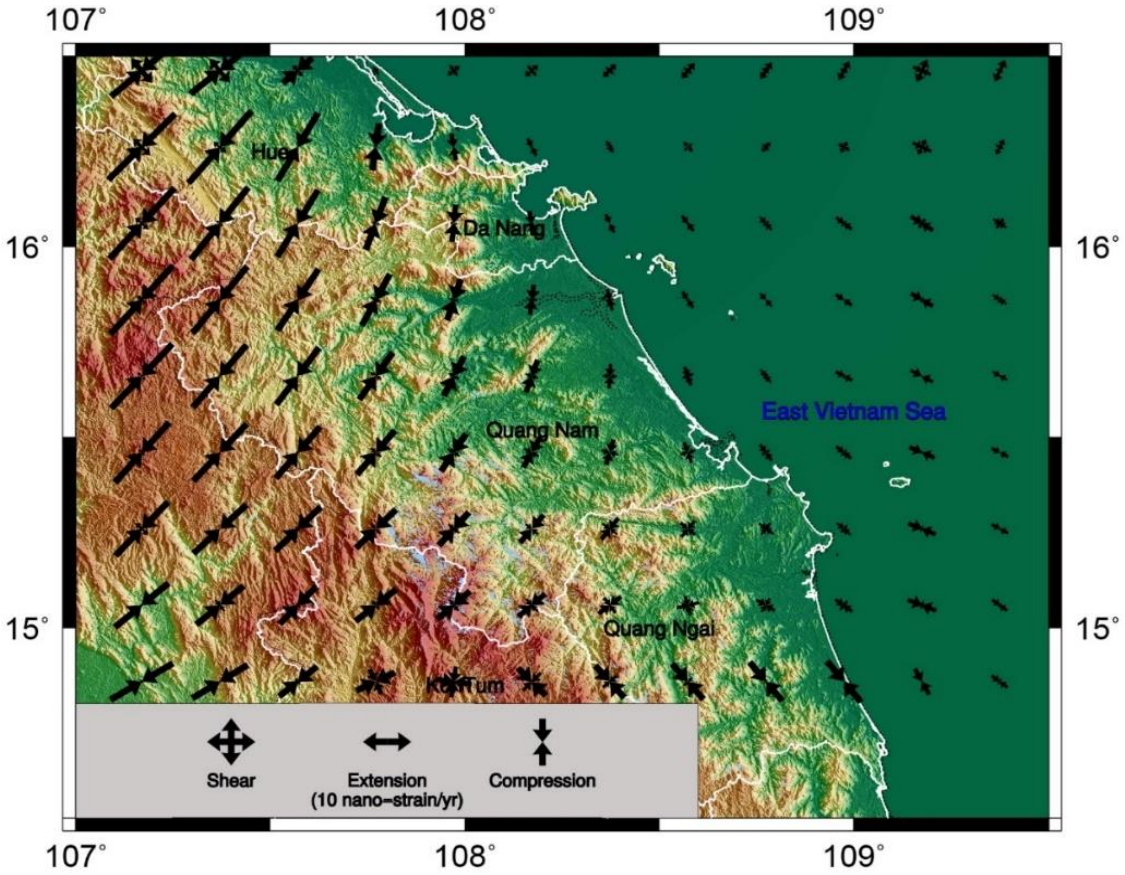

Figure 4. Map of the Present Tectonic Strain rate in the Main Region of Quang Nam - Quang Ngai and surrounding regions

3.2. Rotational Strain rate

The rotational strain rate calculated from the interpolated displacement velocity is detailed in Table 2. Rotational strain rates are generally less than 10 nano-radian/year. The rotational strain rates derived from the interpolated displacement rates provide insight into the rotational trends in the study area (Fig. 5). The region with the highest rotational velocity is west and south of the study area. Overall, the study area experiences a clockwise rotational strain rate, with the central northern coastal region exhibiting a counterclockwise rotational strain rate (Fig. 5) with a magnitude of less than 3 nano-radian/year.

3.3. Magnitude of strain

The magnitude of the strain (IIE) was calculated for each square cell in the interpolated displacement velocity field to obtain a more detailed strain rate picture. The magnitude of the strain is computed at the center of each square cell with dimensions of 0.2°×0.2°. Subsequently, these values are interpolated once again using the method of continuous curved surface grid creation with

an adjustable tension factor (SURFACE - GMT program (Wessel and Smith, 2006) with a tension factor of 0.25 and a convergence limit of 0.1 (Fig. 6).

The results allow for identifying areas with varying degrees of strain rate in the study region. The most extensive strain rate is observed northwest of the study area with a magnitude of approximately 7.5 nano-strain/year. Regions with predominantly moderate magnitudes are mainly concentrated in the mainland of Quang Nam, ranging from 1 to 5 nano-strains/year on average. Areas with weak strain rates are primarily concentrated in the coastal vicinity, with magnitudes less than 1 nano-strain/year (Fig. 6).

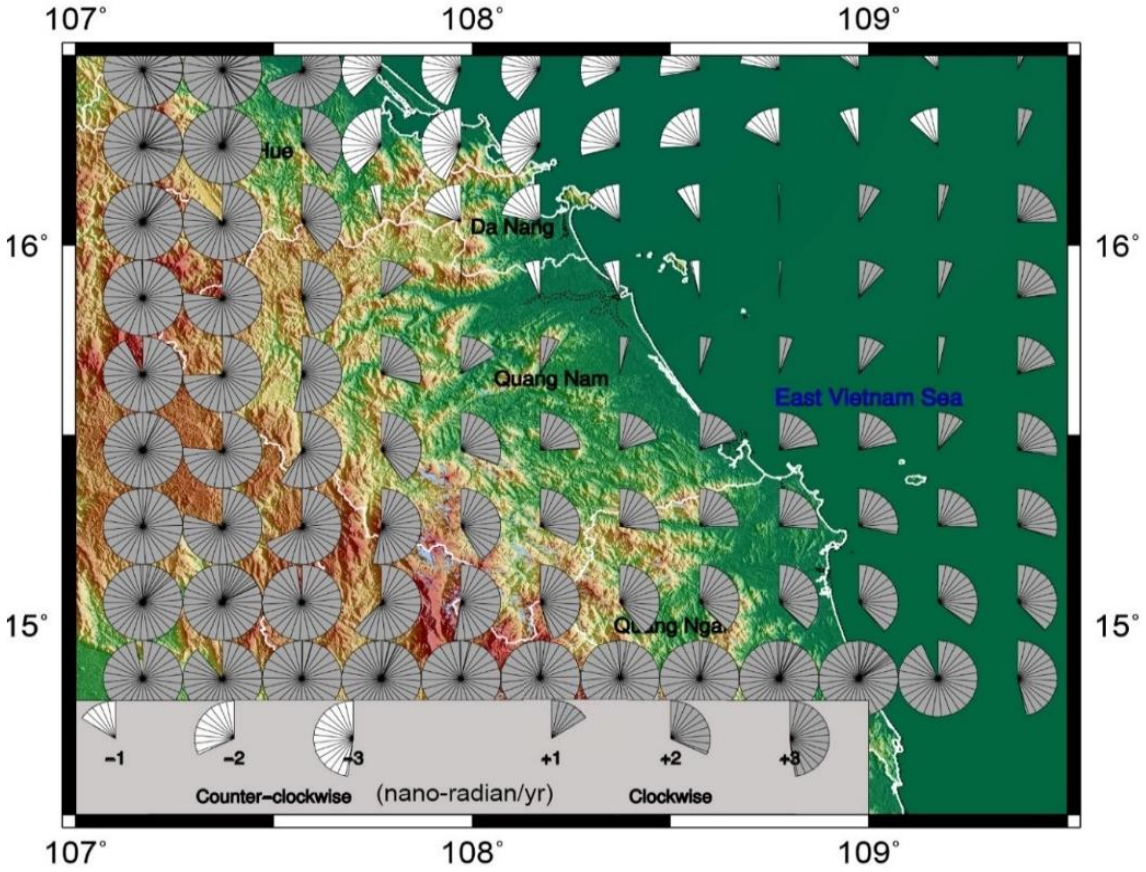

Figure 5. Rotation strain in the Quang Nam - Quang Ngai and surrounding areas

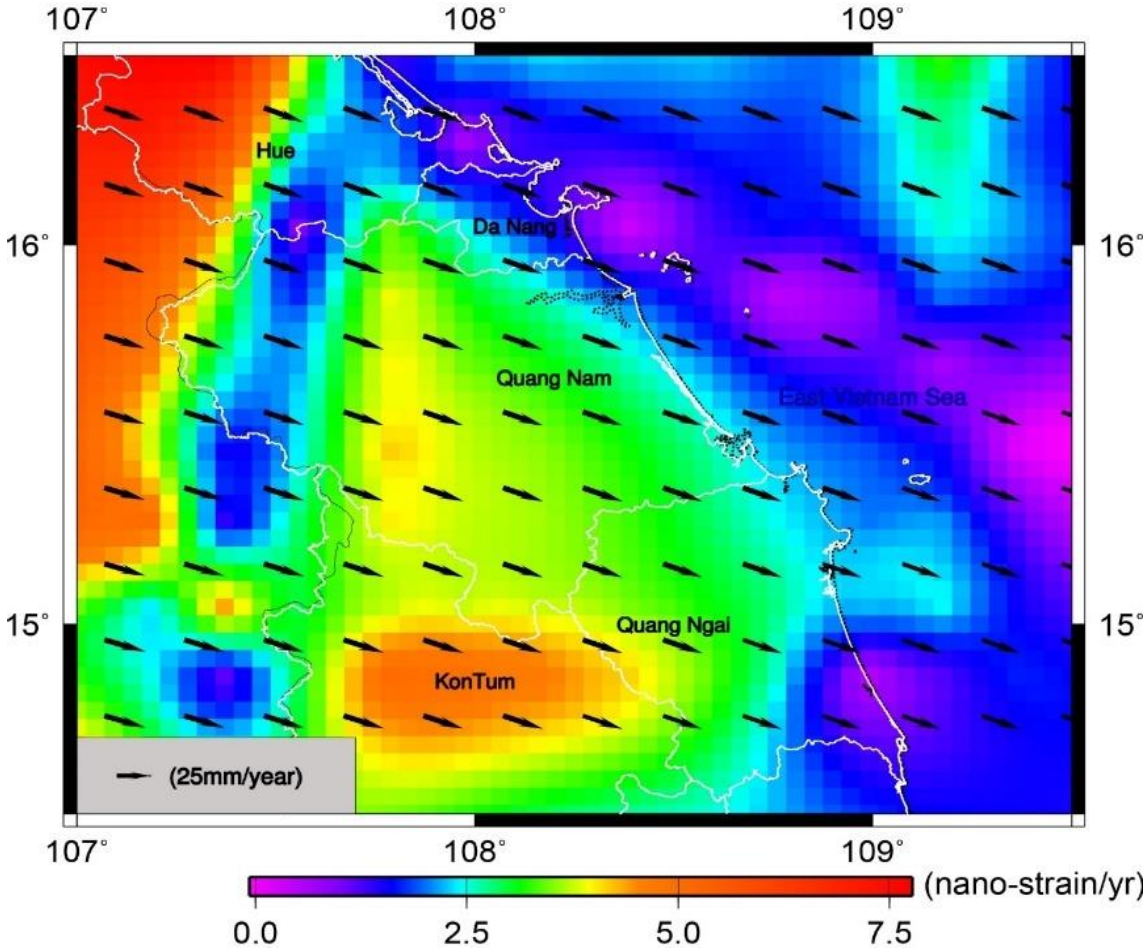

Figure 6. Map of the Second Invariant Magnitude of strain rate in the Southern Quang Nam - Quang Ngai and surrounding areas

3.4. Dilation strain rate

The magnitude of the two-dimensional dilation strain (colored background) is calculated from the interpolated displacement velocity. This value is computed based on the first invariant of the strain tensor. The magnitude of two-dimensional tensile strain is calculated at the center of each square cell with dimensions of 0.2×0.2 degrees. These values are then again interpolated using continuous curved surface grid creation with an adjustable tension factor (SURFACE - GMT program) using a tension factor of 0.25 and a convergence limit of 0.1 (Fig. 7).

Regions with the most significant positive values are primarily concentrated in the offshore eastern part of the study area with rates less than 3 nano-strain/year. Positive values indicate favorable tensile strain for normal faulting. Conversely, negative strain values are observed over much of the mainland area of the study region. Negative values indicate favorable tensile strain for reverse faulting. The most significant negative values of tensile strain velocity are concentrated in the western part of the study area with rates less than -10 nano-strain/year (Fig. 7).

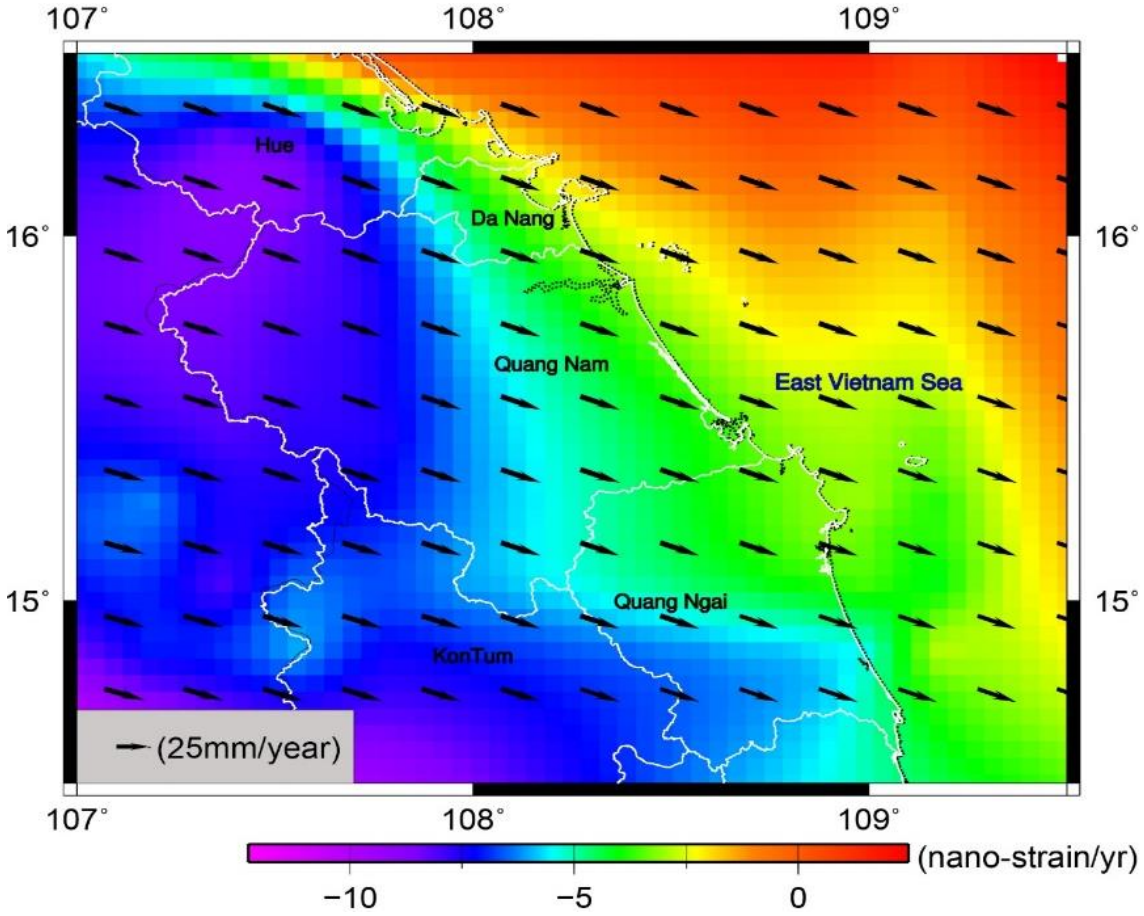

Figure 7. Two-Dimensional Tensile Strain Rate in the study area

3.5. Maximum Shear Strain rate

The magnitude of maximum shear strain (color-coded background with size of plus signs) is computed from the interpolated displacement velocity. The direction of the plus signs indicates the orientation of the maximum shear strain. The magnitude of maximum shear strain is calculated at the center of each square cell with dimensions of 0.2×0.2 degrees. These values are again interpolated using continuous curved surface grid creation with an adjustable tension factor (SURFACE - GMT program) using a tension factor of 0.25 and a convergence limit of 0.1 (Fig. 8).

The region with the highest magnitude of maximum shear strain is located on the mainland to the west of the study area, with a magnitude of approximately 25 nano-strains/year. The direction of the maximum shear strain velocity at this location is primarily along the meridian. The magnitude and orientation of maximum shear strain characterize the localized nature of the shear strain rate, indicating the predominant direction along which shear faulting is most likely to occur (Fig. 8).

Based on the observed absolute displacement velocity data from GPS, the authors calculated the present tectonic strain rates in the study area, yielding the following results:

The principal strain rate in the Quang Nam - Quang Ngai and nearby areas has an average value below 15 nano-strains/year. The dominant mechanism is compressional strain, with compression directed predominantly northeast-southwest over the mainland and mostly northwest-southeast over the sea.

The rotational strain rate mechanism, characterized by clockwise rotation, has speeds below 10 nano-radian/year. The rotation is clockwise in the northern coastal areas, but the rotation speed is less than 3 nano-radian/year.

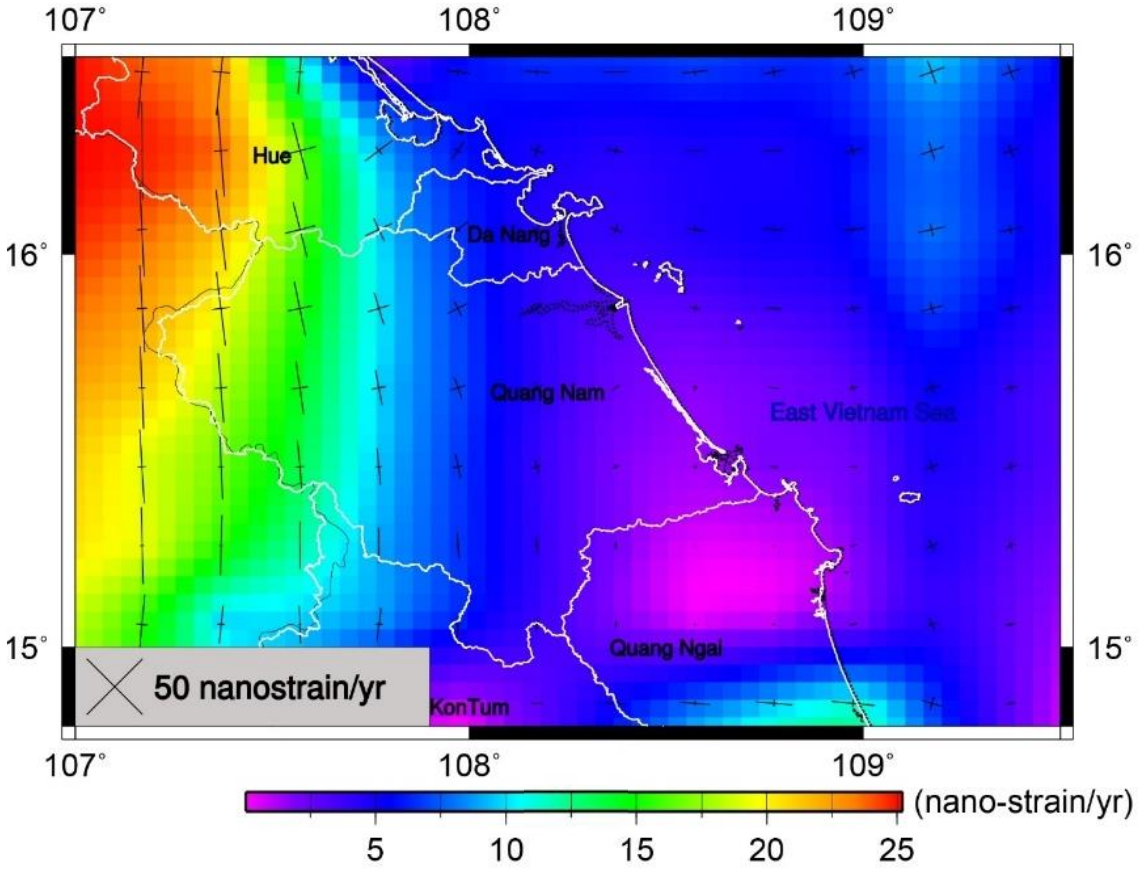

Figure 8. Shear Strain Rate and Maximum Shear Strain in the study area

The magnitude of strain rate, computed from the interpolated displacement velocity using the second invariant of the strain rate tensor, is <7.5 nano-strain/year.

Two-dimensional dilation strain varies from -13 to 3 nano-strain/year.

The magnitude of the maximum shear strain rate is less than 25 nano-strain/year, favoring shear fault development primarily along the meridian.

Based on the synthesis of various documents and GPS displacement data, a present strain rate map at a scale of 1:200,000 for the study area has been established (Fig. 9).

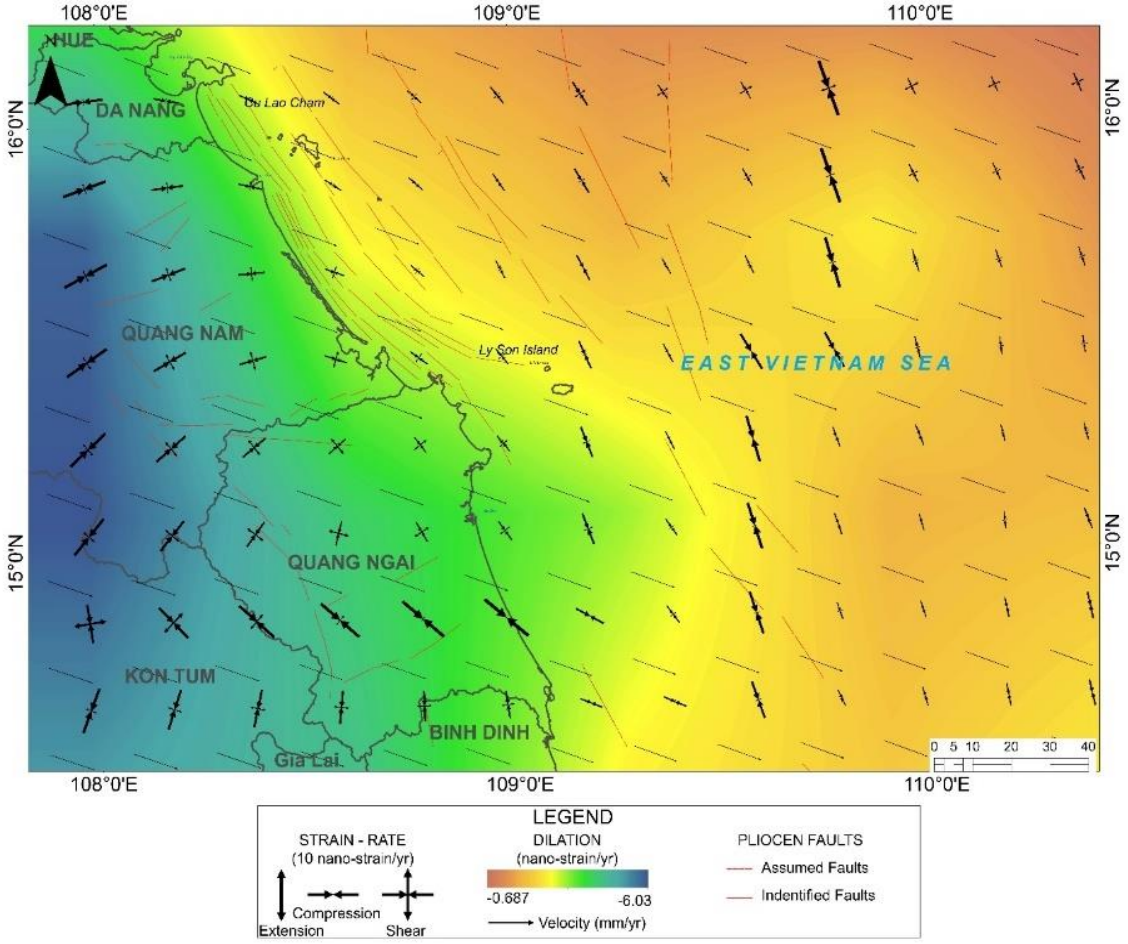

Figure 9. Present Strain Rate Map of the Quang Nam - Quang Ngai and surrounding regions at a Scale of 1:200,000

4. Discussions

The strain rate research has been conducted using various methods, and studies employing geodetic measurements to quantify the strain rate and accumulated strain rate on fault segments have been developed quite diversely. The most common method involves subdividing research areas into closed polygons (often triangles) formed by observation points and calculating the strain rate within each polygon from the displacement velocity of each point (Feigl et al., 1990; Frank, 1966; Shen et al., 1996). This group of methods has also been successfully applied in the Asian region, as evidenced in publications by (Bock et al., 2003), (Calais et al., 2006), (Duong, 2005; Duong et al., 2006), and others. Several computer programs for computing strain rate from GPS data using this approach have been developed, with the noteworthy QOCA software being particularly prominent (Dong et al., 1998).

Another approach utilizes the inverse problem-solving method to map the strain rate field. For instance, (Kreemer et al., 2000) and (Beavan and Haines, 2001) use observed displacements from geodetic networks and strain rates computed from geological and seismic information to solve the inverse problem and determine Euler poles,

minimizing local residuals of strain rate and velocity fields in the reference frames within the region. This computational method often requires time and additional information about fault locations, making it suitable only for quantifying missing slips on known structures and incapable of identifying new structures. Moreover, inverse problem-solving methods rely on assumptions about the mechanical properties of the Earth's crust to relate them to observed strain rates.

The research area exhibits low strain rate conditions, with the principal strain rates being less than 15 nano-strains/year. These results align well with previous publications (Allmendinger et al., 2007; Bock et al., 2003; Calais et al., 2006; Gan et al., 2007; Liu et al., 2007; Phan, 2021; Simons et al., 2007; Stevens and Avouac, 2021; Zhu and Shi, 2011), even though different methods were used, showcasing a significantly higher level of detail. The weakest strain rate is observed in the polygons in the northern central coastal region of the study area. Recent studies on the rotational motion of the Sundaland block (Indochina) (Michel et al., 2001; Simons et al., 2007) align with the results of the rotation strain rate.

The strain rate results indicate stable tectonic activity in the research area, corresponding to longer seismic cycles. Therefore, detailed studies are needed to assess the fractures from the Pleistocene to the present. Another issue in this study is the utilization of interpolated tectonic displacement velocities due to the lack of data from GPS stations within the research area, necessitating detailed studies to evaluate displacement rates for the research area.

5. Conclusions

The Quang Nam - Quang Ngai and surrounding region have a relatively low strain rate field: the average principal strain rate is less than 15 nano-strain/year, with a dominant strike-slip mechanism. The maximum shear strain rate is always less than 25 nano-strains/year. According to the present tectonic deformation mechanism, the study area is favorable for developing predominantly strike-slip faulting.

Following the recommendations of the IAEA, due to the relatively low strain in the Quang Nam - Quang Ngai region, it is essential to assess fault activities from 100,000 to 10,000 years ago.

The characteristics of present tectonic deformation in the study area do not show clear correlations or patterns with geological features, including age, topography, and tectonic faults.

Acknowledgments

This research is funded by the Vietnam Academy of Science and Technology (VAST) under grant number KHCBTĐ.01/21-23; NVCC11.01/22-23 and SKTĐT0.07/23-23.

References

Allmendinger R.W., Reilinger R., Loveless J., 2007. Strain and rotation rate from GPS in Tibet, Anatolia, and the Altiplano. Tectonics, 26.

Beavan J., Haines J., 2001. Contemporary horizontal velocity and strain rate fields of the Pacific-Australian plate boundary zone through New Zealand. J. Geophys. Res, 741–770.

Bock Y., Prawirodirdjo L., Genrich J.F., Stevens C.W., McCaffrey R., Subarya C., Puntodewo S.S.O., Calais E., 2003. Crustal motion in Indonesia from Global Positioning System measurements. Journal of Geophysical Research: Solid Earth, 108, 2367. Doi: 2310.1029/2001JB000324.

Calais E., Dong L., Wang M., Shen Z., Vergnolle M., 2006. Continental deformation in Asia from a combined GPS solution. Geophysical Research Letters, 33, 6.

Chamote-Rooke N., Pichon X.L., 1999. GPS determined eastward Sundaland motion with respect to Eurasia confirmed by earthquake slip vectors at Sunda and Philippine Trenches. Earth and Planetary Science Letters, 173, 439–455.

Dawson J., Hu G., 2010. Improving the geodetic infrastructure of the Asia-Pacific region. XXIV FIG International Congress.

Dao M.D., Vu Cao M., Hoang Hai Y., Nguyen The L., Do Minh D., 2023. Analysis of landslide kinematics integrating weather and geotechnical monitoring data at Tan Son slow moving landslide in Ha Giang province. Vietnam J. Earth Sci., 45(2), 131–146. https://doi.org/10.15625/2615-9783/18204.

Doan V.L., Nguyen B.-Q.-V., Nguyen C.C., Nguyen C.T., 2024. Effect of time-variant rainfall on landslide susceptibility: A case study in Quang Ngai Province, Vietnam. Vietnam J. Earth Sci., 46(2), 203–221. https://doi.org/10.15625/2615-9783/20065.

Dong D., Herring T.A., King R.W., 1998. Estimating Regional Deformation from a Combination of Space and Terrestrial Geodetic Data. Journal of Geodesy, 72, 200-214.

Duong C.C., 2005. Applying a two-dimensional deformable parameter model to evaluate horizontal displacement of the Red River fault. Vietnam J. Earth Sci. (in Vietnamese), 27(3), 193–198.

Duong C.C., Yun H.S., Cho Y.M., 2006. GPS measurements of horizontal deformation across the Lai Chau - Dien Bien (Dien Bien Phu) fault, in Northwest of Vietnam, 2002–2004. Earth Planets Space, 58, 523–528.

Feigl K., King R., Jordan T., 1990. Geodetic Measurement of Tectonic Deformation in the Santa Maria Fold and Thrust Belt, California. Journal of Geophysical Research: Solid Earth, 95, 2679–2699.

Frank F.C., 1966. Deduction of earth strains from survey data. Bulletin of the Seismological Society of America, 56, 35–42.

Gan W., Zhang P., Shen Z.K., Niu Z., Wang M., Wan Y., Zhou D., Cheng J., 2007. Present-day crustal motion within the Tibetan Plateau inferred from GPS measurements. Journal of Geophysical Research: Solid Earth, 112.

Gerald G., Michael H., Robert M.C., Ernesto C., Qizhi C., 2007. Analysis of crustal deformation in Luzon, Philippines using geodetic observations and earthquake focal mechanisms. Tectonophysics, 432, 63–87.

Hao M., Li Y., Zhuang W., 2019. Crustal movement and strain distribution in East Asia revealed by GPS observations. Scientific Reports, 9.

Hsu Y.J., Yu S.B., Simons M., Kuo L.C., Chen H.Y., 2009. Interseismic crustal deformation in the Taiwan plate boundary zone revealed by GPS observations, seismicity, and earthquake focal mechanisms. Tectonophysics, 479, 4–18.

Hu X., Wang Q., Ma Q., Du X., 2007. Research and application of regional no-net-rotation reference frame. Journal of Geodesy and Geodynamics, 27, 52–60.

Isaaks E.H., Srivastava R.M., 1989. An Introduction to Applied Geostatistics. Oxford University Press, New York.

Iwakuni M., Kato T., Takiguchi H., Nakaegawa T., Satomura M., 2004. Crustal deformation in Thailand and tectonics of Indochina peninsula as seen from GPS observations. Geophysical Research Letters, 31, 4.

King R., Shen F., Burchfiel B., Royden L., Wang E., Chen Z., Liu Y., Zhang X., Zhao J., Li Y., 1997. Global Positioning System measurements from eastern Tibet and their implications for India/Eurasia intercontinental deformation. Geology, 25, 179–182.

Kreemer C., Haines J., Holt W.E., Blewitt G., Lavallee D., 2000. On the determination of a global strain rate model. Earth, Planets and Space, 52, 765–770.

Liao C., Wu J., 2009. Study on characteristics of present-day crustal movement in Beibu Gulf area. Journal of Geodesy and Geodynamics, 29, 22–26.

Liem N. V., Trinh P.T., Phong T.V., Lien V.T.H., Huong N.V., Xuyen N.Q., Thanh B.N., Hao D.V., Pham B.T., Dung N.V., Dang V.K., An V.H., 2021. Pliocene - present tectonics and strain rate in Ninh Thuan region and surrounding continental shelf. Vietnam J. Earth Sci., 43(1), 33–56. https://doi.org/10.15625/0866-7187/15694.

Liu M., Yang Y., Shen Z., Wang S., Wang M., Wan Y., 2007. Active tectonics and intracontinental earthquakes in China: The kinematics and geodynamics. Book chapter: Continental Intraplate Earthquakes: Science, Hazard, and Policy Issues. The Geological Society of America. https://doi.org/10.1130/2007.2425(19).

Michel G.W., Yue Q.Y., Sheng Y.Z., Christoph R., Matthias B., Ewald R., Wim S., Boudewijn A., Christophe V., Nicolas C.R., Xavier L.P., Peter M., Saskia M., 2001. Crustal motion and block behavior in SE-Asia from GPS measurements. Earth and Planetary Science Letters, 187, 239–244.

Mustafar M.A., Simons W.J.F., Tongkul F., Satirapod C., Omar K.M., Visser P.N.A.M., 2017. Quantifying deformation in North Borneo with GPS. Journal of Geodesy, 91, 1241–1259.

Nguyen H.D, Kha Dang D., Nhu Nguyen Y., Pham Van C., Hai Truong Q., Thanh Bui Q., Ionut Petrisor A., 2023. A framework for flood depth using hydrodynamic modeling and machine learning in the coastal province of Vietnam. Vietnam J. Earth Sci., 45(4), 456–478. https://doi.org/10.15625/2615-9783/18644.

Nguyen H.V., 2012. Characteristics of deformation, present stress field, and their relationship with geological hazards in Vietnam territory and neighboring areas, Present Tectonic department. Institute of Geological Sciences, Hanoi.

Pearson C., McCaffrey R., Elliott J.L., Snay R., 2010. HTDP 3.0: software for coping with coordinate changes associated with crustal motion. Journal of Surveying Engineering, 136, 80–90.

Pham VT., Le Hong L., Tran Thanh N., Nguyen Quoc P., Phan Trong T., Dinh Thi Q., Dao Minh D., Nguyen Chau L., Nguyen Hai C., 2023. Mechanism and numerical simulation of a rapid deep-seated landslide in Van Hoi reservoir, Vietnam. Vietnam J. Earth Sci., 45(3), 357–373. https://doi.org/10.15625/2615-9783/18539.

Phan T.T., et al., 2010a. Research of recent tectonic activities, present tectonics, and geodynamics of the East Vietnam Sea, scientific basis for predicting related geological hazards and proposing preventive solutions, National project report (in Vietnamese), Code: KC.09.11/06-10. Institute of Geological Sciences, Hanoi.

Phan T.T., et al., 2010b. Research of the relationship between the oil spill risk and natural geological events in the East Vietnam Sea, National project report (in Vietnamese), code: KC.09.11BS/06-10. Institute of Geological Sciences, Hanoi.

Phan T.T., et al., 2013. Assessment of tectonic gradients in the late Pleistocene - present time in the prospective area for the construction of the Ninh Thuan nuclear power plant, National project report (in Vietnamese) (NAFOSTED), code: 03/2012.

Phan T.T., et al., 2021. Research of Pliocene - Present tectonic movements in islands and Vietnam continental shelve to assess geological hazards, National project report (in Vietnamese), code: KC.09.22/16-20. Institute of Geological Sciences, Hanoi.

Phan T.T., Ngo L.V., Nguyen H.V., Tran P.V., Bui T.V., Nguyen V.T., Nguyen D.T., Hoang V.Q., Nguyen X.Q., Nguyen H.T., Bui T.T., Tran H.Q., 2015a. Results of GPS measurements during the period 2012-2013 in the Central Highlands region and modern tectonic deformation. VNU Journal of Science: Earth and Environmental Sciences (in Vietnamese), 31, 1–13.

Phan T.T., Ngo L.V., Tran T.D., Nguyen H.V., Vy H.Q., Bui T.T., Tran P.V., Hoang V.Q., Nguyen X.D., Nguyen T.V., Nguyen D.T., Dinh V.T., Nguyen T.T., Bui T.T., Nguyen V.T., Le M.T., Tran H.Q., 2015b. Present day deformation in the East Vietnam Sea and surrounding regions. Journal of Marine Science and Technology, 15, 105–118.

Phan T.T., Ngo L.V., Vy H.Q., Tran P.V., Nguyen H.V., Nguyen T.V., Nguyen X.Q., Bui V.T., Nguyen D.T., Haong V.Q., Nguyen H.T., Bui T.T., Tran H.Q., 2015c. Present tectonic gradient in the Ninh Thuan region and its vicinity. Vietnam Journal of Marine Science and Technology (in Vietnamese), 15, 209–224.

Shen Z.K., Jackson D.D., Ge B.X., 1996. Crustal deformation across and beyond the Los Angeles basin from geodetic measurements. Journal of Geophysical Research: Solid Earth, 101, 27957–27980.

Shen Z.K., Lu J., Wang M., Burman R., 2005. Contemporary crustal deformation around the southeast borderland of the Tibetan Plateau. Journal of Geophysical Research, 110.

Simons W.J.F., Socquet A., Vigny C., Ambrosius B.A.C., Haji S.A., Chaiwat P., Subarya C., Sarsito D.A., Matheussen S., Morgan P., Spakman W.,

2007. A decade of GPS in Southeast Asia: Resolving Sundaland motion and boundaries. Journal of Geophysical Research: Solid Earth, 112, 20.

Stevens V.L., Avouac J.-P., 2021. On the relationship between strain rate and seismicity in the India-Asia collision zone: implications for probabilistic seismic hazard. Geophysical Journal International, 226, 220–245.

Tran P.V., 2016. Characteristics of modern tectonic deformation in the Khanh Hoa - Binh Thuan region and vicinity based on GPS displacement data. Hanoi University of Science, VNU, Hanoi.

Tran T.D., Nguyen Y.T., 2004. Modern Earth crust movement in the territory of Vietnam based on GPS measurements. Vietnam J. Earth Sci. (in Vietnamese), 26(4), 579–586.

Tregoning P., Brunner F., Bock Y., Puntodewo S., McCaffrey R., Genrich J., Calais E., Rais J., Subarya C., 1994. First geodetic measurement of convergence across the Java trench. Geophysical Research Letters, 21, 2135–2138.

Wang Q., Zhang P.Z., Freymueller J.T., Bilham R., Larson K.M., Lai X., You X., Niu Z., Wu J., Li Y., Liu J., Yang Z., Chen Q., 2001. Present-day crustal deformation in China constrained by Global Positioning System measurements. Science, 294, 574–577.

Wessel, Smith W.H.F., 2006. GMT Technical Reference and Cookbook, version 4.1.2, p.164.

Yu S.B., Hsu Y.J., Bacolcol T., Yang C.C., Tsai Y.C., Solidum R., 2011. Present-day crustal deformation along the Philippine Fault in Luzon, Philippines. Journal of Asian Earth Sciences, 65, 64–74.

Zhu S., Shi Y., 2011. Estimation of GPS strain rate and its error analysis in the Chinese continent. Journal of Asian Earth Sciences, 40(1), 351-362.